CHEMISTRY OF MATERIALS
Article

Chem. Mater. **2009,** *21,* 5443–5455 5443
DOI:10.1021/cm902123m

Lanthanide Oxide Thin Films by Metalorganic Chemical Vapor Deposition Employing Volatile Guanidinate Precursors

Andrian P. Milanov,[†] Teodor Toader,[∥] Harish Parala,[†] Davide Barreca,[‡] Alberto Gasparotto,[§] Claudia Bock,[∥] Hans-Werner Becker,[⊥] Divine K. Ngwashi,[○] Richard Cross,[○] Shashi Paul,[○] Ulrich Kunze,[∥] Roland A. Fischer,[†] and Anjana Devi*[,†]

[†]*Inorganic Chemistry II, Ruhr-University Bochum, 44801 Bochum, Germany,* [‡]*CNR-ISTM and INSTM, Department of Chemistry, Padova University, Via Marzolo, 1, 35131 Padova, Italy,* [§]*Department of Chemistry, Padova University and INSTM, Via Marzolo, 1, 35131 Padova, Italy,* [∥]*Institute for Electronic Materials and Nanoelectronics, Ruhr-University Bochum, 44801 Bochum, Germany,* [⊥]*Dynamitron-Tandem-Laboratorium (DTL) of RUBION, Ruhr-University Bochum, 44801 Bochum, Germany, and* [○]*Emerging Technologies Research Centre, De Montfort University, Leicester, LE1 9BH, U.K.*

Received July 13, 2009. Revised Manuscript Received September 8, 2009

The application of two novel metalorganic complexes, namely the isostructural *tris*(*N*,*N*'-diisopropyl-2-dimethlyamido-guanidinato)gadolinium(III) (**1**) and *tris*(*N*,*N*'-diisopropyl-2-dimethlyamido-guanidinato)dysprosium(III) (**2**) as precursors for metalorganic chemical vapor deposition (MOCVD) of Gd_2O_3 and Dy_2O_3 is discussed. On the basis of the detailed thermal gravimetric analysis (TGA) and isothermal TGA studies, both the precursors are very volatile and able to deliver continuous mass transport into the gas phase. The extraordinary thermal stability of the precursors was revealed by nulcear magnetic resonance (NMR) decomposition studies. Depositions were carried out in the presence of oxygen at reduced pressure and varying the substrate temperature in the range 300−700 °C. Uniform films with reproducible quality were deposited on Si(100) and Al_2O_3(0001) substrates over the entire temperature range. Employing a multitechnique approach (XRD, SEM, AFM, EDX, XPS, RBS, SNMS, $C-V$), variations of the growth characteristics and film properties with deposition temperature are studied in terms of crystallinity, structure, surface roughness, composition, and electrical properties.

Introduction

Among the wide range of lanthanide oxide materials, gadolinium oxide (Gd_2O_3), and dysprosium oxide (Dy_2O_3) show a variety of attractive features for applications in various fields of technology. They have received a lot of attention lately as alternative gate dielectrics because of their high dielectric constants [$k(Gd_2O_3) = 16$, $k(Dy_2O_3) = 14-18$], large band gaps [$E_g(Gd_2O_3) = 5.6$ eV; $E_g(Dy_2O_3) = 4.9$ eV] and high thermodynamic stability.[1−3] In addition, the close lattice match to Si offers the possible advantage to grow epitaxial films, which probably can eliminate problems related to grain boundaries in polycrystalline films. While thin films of Gd_2O_3 have been projected as promising passivation layer for GaAs(100) surface,[4] Dy_2O_3 is an emerging material for replacing Si_3N_4 in future metal-oxide-high-*k*-oxide-silicon (MOHOS) capacitors[5] and as a capping layer on SiON in Ni-fully-silicide (FUSI) *n*-metal-oxide-semiconductor field-effect transistor (MOSFETs).[6] Further important applications in optics are enabled by their large band gaps, high refractive indices, and extended spectral transparency over ultraviolet (UV) to infrared (IR).[7,8] The thermodynamic stability and the refractory nature of these materials make them suitable as protective and corrosion resistive coatings.[9,10] In a broader sense, these materials are also components in superconducting[11] and thermoelectric oxides,[12,13] as well as solid electrolytes for intermediate-temperature solid-oxide fuel cells (SOFCs).[14,15]

Such a broad range of potential applications has enhanced the research activities to grow high quality thin

*Author e-mail address: anjana.devi@rub.de.

(1) Wilk, G. D.; Wallace, R. M.; Anthony, J. M. *J. Appl. Phys.* **2001**, *89*, 5243.
(2) Leskelä, M; Ritala, M. *J. Solid State Chem.* **2003**, *171*, 170.
(3) Päiväsaari, J.; Putkonen, M.; Niinistö, L. *Thin Solid Films* **2005**, *472*, 275, and references therein .
(4) Hong, M.; Kwo, J.; Kortan, A. R.; Mannearts, J. P.; Sergent, A. M. *Science* **1999**, *283*, 1897.
(5) Hsu, H.; Chang, I. Y.; Lee, J. Y. *IEEE Electron Device Lett.* **2007**, *28*(11), 964.
(6) Yu, H. Y.; Chang, S. Z.; Veloso, A.; Lauwers, A.; Adelmann, C.; Onsia, B.; Lehnen, P.; Kauerauf, T.; Brus, S.; Yin, K. M.; Absil, P.; Biesemans, S. *IEEE Electron Device Lett.* **2007**, *28*(11), 957.
(7) Sahoo, N. K.; Senthikumar, M.; Thakur, S.; Bhattacharyya, D. *Appl. Surf. Sci.* **2002**, *200*, 219.
(8) Dakhel, A. A. *J. Opt. A: Pure Appl. Opt.* **2001**, *3*, 452.
(9) Bonnet, G.; Lachkar, M.; Colson, J. C.; Larpin, J. P. *Thin Solid Films* **1995**, *261*, 31.
(10) Bonnet, G.; Lachkar, M.; Larpin, J. P.; Colson, J. C *Solid State Ionics* **1994**, *72*, 344.
(11) MacManus-Driscoll, J. L. *Annu. Rev. Mater. Sci.* **1998**, *28*, 421, and references therein .
(12) Shibasaki, S.; Terasaki, I. *J. Phys. Soc. Jpn.* **2006**, *75*(2), 024705.
(13) Hao, H.; Chen, C.; Pan, L.; Gao, J.; Hu, X. *Physica B* **2007**, *387* (1−2), 98.
(14) Song, H. Z.; Wang, H. B.; Zha, S. W.; Peng, D. K.; Meng, G. Y. *Solid State Ionics* **2003**, *156*, 249.
(15) Song, H.; Xia, C.; Meng, G.; Peng, D. *Thin Solid Films* **2003**, *434*, 244.

Published on Web 10/21/2009

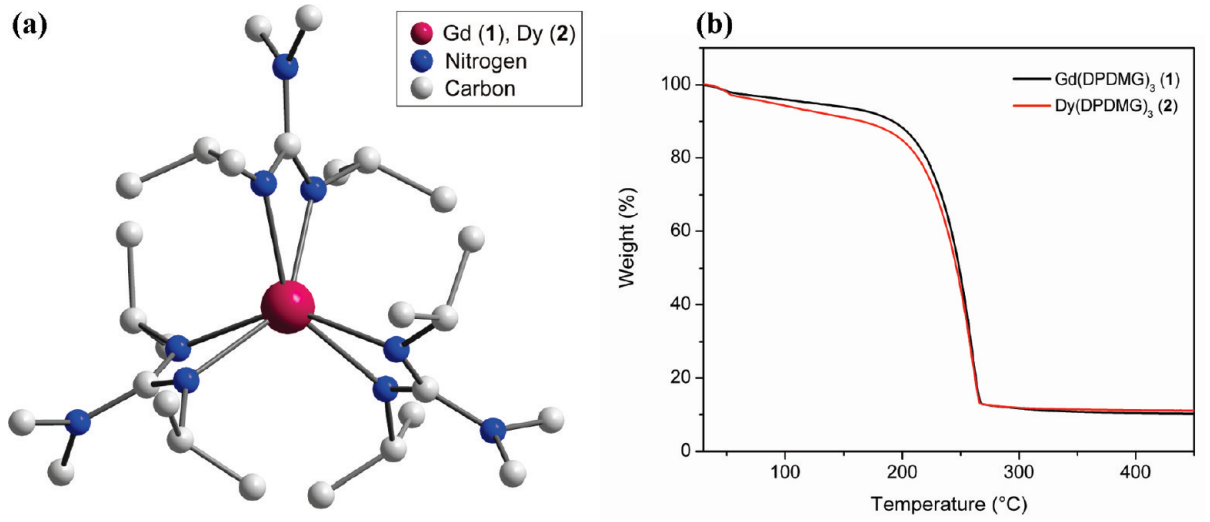

Figure 1. (a) Molecular structure in the solid state and (b) TGA curves of $Gd(DPDMG)_3$ (**1**) and $Dy(DPDMG)_3$ (**2**).

films. Primary physical vapor deposition (PVD) techniques such as ultrahigh vacuum vapor deposition,[16,17] thermal and electron beam evaporation,[18−21] and (radio frequency (rf)) magnetron sputtering[22−24] have been employed to grow Gd_2O_3 and Dy_2O_3 thin films. However, metalorganic chemical vapor deposition (MOCVD) and atomic layer deposition (ALD) are preferred over PVD techniques when there is a necessity to have large area deposition, good composition control, and uniform step coverage on nonplanar device geometries, all of which are the advantages of these two techniques.[25,26]

Compared to other functional oxides, there are very limited reports available on the MOCVD and ALD growth of Gd_2O_3 and Dy_2O_3 thin films, which is primarily due to the lack of suitable precursors with appropriate thermal characteristics in terms of volatility, stability, and decomposition characteristics. In the case of MOCVD of Gd_2O_3, β-diketonate complexes like $[Gd(thd)_3]_x$·tetraglyme (thd = 2,2,6,6-tetramethylheptane-3,5-dionate; tetraglyme = tetraethylene glycol dimethyl ether) were used (T_{sub} = 250−700 °C), but the quality of the obtained films was poor probably due to precursor sintering and partial decomposition at the evaporation temperature (190−230 °C).[27] $[Gd(mmp)_3]_x$ (mmp = 1-methoxy-2-methyl-2-propanolate) is another precursor which has been used, but it was found to undergo oligomerization leading to a low volatile oxo-bridged $[Gd(mmp)_2]_2O$ complex that required vaporization temperature above 170 °C. However, using a mixture of $[Gd(mmp)_3]_x$ and tetraglyme, Gd_2O_3 films were deposited by liquid injection (LI) MOCVD (T_{sub} = 300−600 °C).[28] The films were reported to be nearly carbon free, but with a large oxygen excess (O:Gd ratio = 1.7−2.0) and significant chlorine contamination (up to 7%). In another report, Gd_2O_3 thin films were grown using Gd(acac)$_3$·Phen (acac = pentane-2,4-dionate; Phen = phenanthroline) as the precursor (T_{sub} = 450−800 °C).[29] In this case too, high evaporation temperatures (> 200 °C) were required and the resulting films were highly contaminated with carbon. In terms of precursors for Dy_2O_3 thin films, the use of the highly sensitive organometallic (COT)Cp*Dy (COT = 1,3,5-cyclooctatriene; Cp* = 1,2,3,4,5-pentamethylcyclopentadiene) by plasma-enhanced chemical vapor deposition (PECVD) led to film growth at 350−400 °C, but carbon contaminated, poor quality films were obtained.[30] The methoxy-propanolate $[Dy(mmp)_3]_x$[31] and the β-diketonate Dy(EDMDD)$_3$ (EDMDD = 6-ethyl-2,2-dimethyl-3,5-decanedionate)[32] were successfully used for LI-MOCVD of Dy_2O_3. While for the mmp complex significant particle formation and lithium contamination of the film was reported, the films obtained using Dy(EDMDD)$_3$ were found to be of good quality.

(16) Pal, S.; Ray, S. K.; Chakraborty, B. R.; Lahiri, S. K.; Bose, D. N. *J. Appl. Phys.* **2001**, *90*(8), 4103.
(17) Kwo, J.; Hong, M.; Kortan, A. R.; Queeney, K. L.; Chabal, Y. J.; Opila, R. L.; Muller, D. A.; Chu, S. N. G.; Sapjeta, B. J.; Lay, T. S.; Mannaerts, J. P.; Boone, T.; Krautter, H. W.; Krajewski, J. J.; Sergnt, A. M.; Rosamilia, J. M. *J. Appl. Phys.* **2001**, *89*(7), 3920.
(18) Koleshko, V. M.; Babushkina, N. V. *Thin Solid Films* **1979**, *62*, 1.
(19) Dakhel, A. A. *J. Alloys Compd.* **2006**, *422*, 1.
(20) Landheer, D.; Gupta, J. A.; Sproule, G. I.; McCaffrey, J. P.; Graham, M. J.; Yang, K.- C; Lu, Z.- H.; Lennard, W. N. *J. Electrochem. Soc.* **2001**, *148*(2), G29.
(21) Bhattacharyya, D.; Biswas, A. *J. Appl. Phys.* **2005**, *97*, 053501.
(22) Chang, S.- C.; Deng, S.- Y.; Lee, J. Y.-M. *Appl. Phys. Lett.* **2006**, *89*, 053504.
(23) Chiu, F.- C. *J. Appl. Phys.* **2007**, *102*, 044116.
(24) Hwang, Y.- R.; Chang, I. Y.; Wang, M.; Lee, J. Y. *Integr. Ferroelectr.* **2008**, *97*, 111.
(25) Jones, A. C; Hitchman, M. L *Chemical Vapor Deposition: Precursors, Processes and Applications*; Royal Society of Chemistry: Cambridge, 2009; Chapter 5.
(26) Leskelä, M.; Kukli, K.; Ritala, M. *J. Alloys Compd.* **2006**, *418*, 27.
(27) McAleese, J; Plakatouras, J. C.; Steele, B. C. H. *Thin Solid Films* **1996**, *286*, 64.
(28) Aspinall, H. C.; Gaskell, J. M.; Loo, Y. F.; Jones, A. C.; Chalker, P. R.; Potter, R. J.; Smith, L. M.; Critchlow, G. W. *Chem. Vap. Deposition* **2004**, *10*(6), 301.
(29) Singh, M. P.; Thakur, C. S.; Shalini, K.; Banerjee, S.; Bhat, N.; Shivashankar, S. A. *J. Appl. Phys.* **2004**, *96*(10), 5631.
(30) Weber, A.; Suhr, H.; Schumann, H.; Köhn, R.-D. *Appl. Phys. A: Mater. Sci. Process.* **1990**, *51*, 520.
(31) Van Elshocht, S.; Lehnen, P.; Sitzinger, B.; Abrutis, A.; Adelmann, C.; Brijs, B.; Caymax, M.; Conard, T.; De Gendt, S.; Franquet, A.; Lohe, C.; Lukosius, M.; Moussa, A.; Richard, O.; Williams, P.; Witters, T.; Zimmerman, P.; Heyns, M. *J. Electrochem. Soc.* **2006**, *153*(9), F219.
(32) Thomas, R.; Ehrhart, P.; Roeckerath, M.; Van Elshocht, S.; Rije, E.; Luysberg, M.; Boese, M.; Schubert, J.; Caymax, M.; Waser, R. *J. Electrochem. Soc.* **2007**, *154*(7), G147.

Taken together, these observations highlight the need for alternative Gd and Dy CVD precursors with improved shelf life and mass transport properties. Following our successful studies on using guanidinates as effective chelating ligands in combination with transition metals,[33−35] we recently reported the synthesis of a series of monomeric *tris*-guanidinato complexes Ln[(N^iPr)$_2$-CNR_2]$_3$ (Ln = Y, Gd, and Dy; R = Me, Et, ^{i}Pr), which showed excellent characteristics in terms of thermal stability and volatility.[36] In this study, we report on the detailed evaluation of the thermal properties of two guanidinato complexes, namely *tris*(*N*,*N*'-*di*iso*p*ropyl-2-*dim*ethylamido-*g*uanidinato)gadolinium(III) and *tris*(*N*,*N*'-*di*iso*p*ropyl-2-*dim*ethylamido-*g*uanidinato)dysprosium-(III) [later referred as Ln(DPDMG)$_3$, Ln = Gd (**1**) or Dy (**2**), Figure 1a] in view of their application as precursors for MOCVD and ALD of rare-earth based materials. In addition, in this work, compounds **1** and **2** were successfully applied as Gd and Dy precursors for the MOCVD of Gd_2O_3 and Dy_2O_3, respectively. Therefore, the attention is also devoted to the film structural, morphological, compositional, and electrical characterization, highlighting the most relevant film properties in relation to the distinct advantages of the proposed precursors.

Experimental Section

Precursor Synthesis. The complexes *tris*(*N*,*N*'-diisopropyl-2-dimethylamido-guanidinato)gadolinium(III) [Gd(DPDMG)$_3$] (**1**) and *tris*(*N*,*N*'-diisopropyl-2-dimethylamido-guanidinato)-dysprosium(III) [Dy(DPDMG)$_3$] (**2**) were synthesized following the procedure published earlier.[36] All reactions were performed employing a conventional vacuum/argon line using standard Schlenk techniques. The scale up of precursors was done in batches of 10−15 g. The precursors were purified by sublimation in vacuum (120 °C/5×10^{-2} mbar). The purity of the precursors was confirmed using NMR and elemental analysis recorded on a Bruker Advance DPX 250 spectrometer and CHNSO Vario EL analyzer, respectively. The preparation of samples for analysis was carried out in an argon-filled glovebox (MBraun). Thermogravimetric analysis (TGA) data were obtained on a Seiko TG/DTA 6300S11 instrument. The measurements were performed in aluminum crucibles closed with an Al lid with a hole (area 1.5 mm^2) using approximately 10 mg of sample. The heating rate was 5 °C/min and a nitrogen flow of 300 mL/min was used. The thermal behavior of **1** and **2** was further investigated using isothermal TGA studies. For each study, the sample was held at a fixed temperature and the mass loss was measured for 720 min (12 h). NMR decomposition measurements were performed to further investigate the long-term thermal stability of the precursors. Therefore C_6D_6 solutions of the compounds, sealed in heavy walled NMR tubes, were heated in an oven for a long period of time. Periodically, the tubes were cooled to room temperature and ^{1}H NMR spectra were recorded. By comparing the integral areas of its NMR peaks, normalized to the solvent peak (C_6D_5H), the amount of undecomposed compound was estimated. From the linear fit of the obtained curves, the half-life of the compounds at the corresponding temperature was calculated.

Thin Film Deposition. A home-built horizontal cold-wall MOCVD reactor operating under reduced pressure was used for film growth.[37] Deposition of thin films was studied in the temperature range 300−700 °C. Gd_2O_3 and Dy_2O_3 films were deposited on *p*-doped Si(100) and Al_2O_3(0001) (1.4 cm×1 cm) at 1 mbar reactor pressure. Prior to deposition, the substrates were ultrasonically cleaned in acetone and ethanol, rinsed with deionized water (Millipore water purification system), and dried under argon stream. For Si(100), the native SiO_2 layer was not removed prior to deposition. High-purity nitrogen (99.9999%, 50 sccm) was used as carrier gas and oxygen (99.998%, 50 sccm) as the oxidant, and the flow rates were monitored using mass flow controllers (MKS). About 100 mg of the precursor was used for each deposition, and the vaporizer temperature was maintained at 120 °C. Generally, the standard deposition time used during MOCVD was 15 min. However, experiments with deposition time in the range 5−30 min were also performed to verify the obtained results and when a concrete film thickness was required.

Thin Film Characterization. Crystallinity of the films was investigated by carrying out X-ray diffraction (XRD) analysis in a Bruker AXS D8 Advance diffractometer, using Cu Kα radiation (1.5418 Å). Surface morphology was studied with scanning electron microscopy (SEM; LEO; Zeiss) and atomic force microscopy (AFM; Nanoscope Multimode III AFM; Digital Instruments). The AFM measurements on Gd_2O_3 were performed in contact mode, whereas for Dy_2O_3 tapping mode was used. The thin films growth rates at given temperature were calculated using the film thicknesses, which were obtained from the cross-sectional SEM micrographs and verified by ellipsometric measurements. Film composition was determined by X-ray photoelectron spectroscopy (XPS), Rutherford backscattering spectrometry (RBS), and secondary neutral mass spectrometry (SNMS) analysis. The XPS spectra were recorded on a Perkin-Elmer Φ 5600ci spectrometer at a pressure lower than 10^{-9} mbar, using a monochromatized Al Kα excitation source (1486.6 eV). The spectrometer was calibrated by assigning to the Au 4f7/2 line the binding energy (BE) of 84.0 eV with respect to the Fermi level. The BE shifts were corrected assigning to the C 1s line of adventitious carbon a value of 284.8 eV. The estimated standard deviation for BEs was ±0.2 eV. The atomic compositions were evaluated using sensitivity factors provided by Φ V5.4A software. The Gd(Dy) 4d signals were used in the quantitation instead of the more intense Gd(Dy) 3d ones, since the latter present an appreciable BE difference with respect to the O and C peaks. This feature would imply the analysis of photoelectrons with different escape depths, yielding thus an uncorrected system composition.[38] Ar^+ sputtering was carried out at 3 kV and 0.5 mA/cm^2 beam current density, with an argon partial pressure of 5×10^{-8} mbar. The sample was introduced directly into the analysis chamber by a fast entry lock system. RBS measurements were performed using an instrument from the Dynamitron Tandem Laboratory (DTL) in Bochum. A beam intensity of about 40−50 nA incident to the sample at a tilt angle of 7° was used. The backscattered particles were

(33) Milanov, A.; Bhakta, R.; Baunemann, A.; Becker, H.-W.; Thomas, R.; Ehrhart, P.; Winter, M.; Devi, A. *Inorg. Chem.* **2006**, *45*, 11008.
(34) Devi, A.; Bhakta, R.; Milanov, A.; Hellwig, M.; Barreca, D.; Tondello, E.; Thomas, R.; Ehrhart, P.; Winter, M.; Fischer, R. A. *Dalton Trans.* **2007**, 1671.
(35) Baunemann, A.; Rische, D.; Milanov, A.; Kim, Y.; Winter, M.; Gemel, C.; Fischer, R. A. *Dalton Trans.* **2005**, 3051.
(36) Milanov, A.; Fischer, R. A.; Devi, A. *Inorg. Chem.* **2008**, *47*(23), 11405.
(37) Devi, A; Rogge, W.; Wohlfart, A.; Hipler, F.; Becker, H.-W.; Fischer, R. A. *Chem. Vap. Deposition* **2000**, *6*, 245.
(38) Briggs, D.; Seah, M. *Practical Surface Analysis: Auger and X-ray Photoelectron Spectroscopy*; Wiley: New York, 1990.

Table 1. Summary of the Literature Reported Gd and Dy Precursors, Their Evaporation Temperatures, and the Processes Employed for Film Growth

precursor	evaporation conditions	process	ref
$Gd(acac)_3$•Phen	200 °C/2.67 mbar	MOCVD	29
$[Gd(thd)_3]_x$•tetraglyme	190−230 °C/ 2.67 mbar	MOCVD	27
$[Gd(mmp)_3]_x$•tetraglyme	> 170 °C/2−3 mbar	LI-MOCVD	28
(COT)Cp*Dy	160 °C/0.2 mbar	PECVD	30
$Dy(EDMDD)_3$	nr[a]	LI-MOCVD	32
$Gd(DPDMG)_3$	95−120 °C/1 mbar	MOCVD	this study
$Dy(DPDMG)_3$	95−120 °C/1 mbar	MOCVD	this study
$Gd(^iPr_2\text{-Me-amd})_3$	140 °C/nr	ALD	40
$(CpMe)_3Gd$	110 °C/2−3 mbar	ALD	41
$[Gd(DPM)_3]_x$	195 °C/2−3 mbar	ALD	42
$[Gd(mmp)_3]_x$•tetraglyme	nr	LI-ALD	65

[a] Not reported.

measured at an angle of 160° by an Si detector with a resolution of 16 keV. The stoichiometry of the films was calculated using the program RBX.[39] The composition depth profile of the films was determined by SNMS measurements employing a VG SIMSLABB IIIA instrument [MATS (UK) Ltd.]. The primary ion beam was argon at 10 keV, usually operated at high currents (0.8−1.0 μA) over large areas (0.5−4 mm raster size) depending on the total depth requirements. The current−voltage ($I-V$) and capacitance−voltage ($C-V$) behavior of metal−insulator−semiconductor (MIS) structures (Al/high-k insulator/Si-(100) with Al back contact) were carried using an HP4140B picoammeter and an HP4192A LCR bridge. Voltage sweeps for $C-V$ measurements were carried out, at different frequencies, from inversion to accumulation and back to inversion. The leakage current through the insulator was measured, using an HP4140B picoammeter, prior to any $C-V$ measurements. The dielectric constant (k) of the films was determined using the relation $C=k\mathrm{A}/d$, where $k=\varepsilon_o\varepsilon_r$, ε_o and ε_r are the permittivity of free space and relative permittivity of the dielectric, d is the thickness of the film, A is the Al gate area (7.85×10^{-3} cm^2), and C is the dielectric capacitance (at accumulation) obtained from the 1 MHz $C-V$ curves.

Results and Discussion

Precursor Evaluation. One of the major challenges for a successful MOCVD or ALD process is the availability of suitable precursors exhibiting appropriate chemical and physical properties.[25] The precursors should be pure, volatile, and stable at room temperature for long periods of time (shelf life), and they should not undergo premature decomposition during evaporation or the mass transport process. The precursors used for CVD are generally also applicable for ALD processes, but with some additional requirements. In the latter case, there should be sufficient thermal stability both in the gas phase and on the substrate surface to avoid uncontrolled self-decomposition in the deposition temperature window, which can lead to CVD contributions. In addition, in case of oxide precursors, high reactivity toward water is of great importance, since the use strong oxidizing agents like ozone could decrease device performance.

With these prerequisites in mind, the thermal properties of compounds **1** and **2** for eventual applications in MOCVD and ALD were investigated in detail by TGA, isothermal TGA measurements at different temperatures, and by NMR decomposition studies.

According to TGA (Figure 1b), both compounds exhibit similar thermal behavior corresponding to single step evaporation, which is essential for a good MOCVD and ALD precursor. The temperature onset of volatilization (ca. 220 °C) and the temperature at which the evaporation is completed (ca. 270 °C) are similar for both the compounds. The observed residual masses of ca. 9 wt % are very likely due to the fact that the presented TGA curves were recorded on a TG machine, which is operated at ambient conditions outside a glovebox. For air sensitive compounds like the rare earth guanidinates, this could lead to partial decomposition during the short exposure to air when the crucible is placed on the balance and thus to higher residual masses. In fact a closer look at the TGA curves in Figure 1b shows a weight loss step of ca. 6−7%, which starts already at the beginning of the measurement (ca. 35 °C) and can be attributed to partial precursor decomposition through reaction with ambient air. However, though the main part of the residue observed in the TGA is due to precursor reaction with ambient, some thermal decomposition above 270 °C could not be excluded.

It is noteworthy to mention that, due to the similarities in their thermal properties, one and the same set of deposition conditions during the MOCVD or ALD process could be used for both **1** and **2**. This will allow a direct correlation of the deposition results, whereas any differences in growth behavior will only be caused by the difference in the physicochemical properties of the precursors under the concrete deposition conditions.

The single step evaporation observed in the TG curves implies that the precursors can be sublimed without decomposition. This was verified by carrying out sublimation experiments. It was found that both the precursors could be sublimed quantitatively in the temperature range 90−130 °C under reduced pressure (6×10^{-2} mbar) in a span of a couple of hours without any measurable residue or color change. In addition, gas phase transport experiments at 1 mbar were performed using the MOCVD reactor setup used for film deposition. These experiments revealed that an effective mass transport of **1** and **2** could be achieved at bubbler temperatures between 95 and 120 °C. In comparison, previously proposed Gd and Dy precursors for MOCVD and PECVD require much higher evaporation temperatures (see Table 1).

Beside suitable evaporation behavior, a good MOCVD and ALD precursor should also be able to deliver constant mass transport over a long period of time, thus giving sustainable growth rates. Using isothermal TG studies, the transport properties of both precursors **1** and **2** in the temperature range 100−160 °C at atmospheric pressure were investigated. Irrespective of the adopted temperature, a constant weight loss over a time period as long as 12 h was observed and evaporation rates of 6.17−17.12 μg/min·cm^2 for **1** and 5.7−17.4 μg/min·cm^2 for **2** were obtained from the slope of the curves (see SI 1 in

(39) Kótai, E. *Nucl. Instrum. Methods* **1994**, *B85*, 588.

the Supporting Information). These results clearly show that compounds **1** and **2** are thermally stable at the given temperatures, thus being able to give stable mass transport. A comparison of the vaporization characteristics of compounds **1** and **2** with those of the literature reported molecular sources clearly shows that the present homoleptic Gd and Dy guanidinate complexes are more volatile and thus very promising MOCVD/ALD precursors.

Further, we used NMR decomposition studies in order to assess and quantify the thermal stability, viz. the half-life of the precursors, not only at typical evaporation temperatures (100 and 140 °C), but also at common ALD deposition temperatures (180 and 220 °C). Accordingly, at 140 °C, which is above the sublimation and evaporation temperatures used in the studies described earlier, the half-life of Dy(DPDMG)$_3$ (**2**) is more than 1 y (see SI 2 in the Supporting Information). Even at 220 °C, which is a typical substrate temperature for ALD of lanthanide oxides, precursor **2** is remarkably stable with half-life of ca. 33 h. Due to the strong paramagnetic character of Gd^{3+} in **1**, NMR decomposition studies for this precursor were not possible. However since the TG properties of both precursors **1** and **2** are very similar (see Figure 1 and SI 1), their thermal stabilities should not be that different. This assumption could also be strengthened by the fact that an analogous Y(DPDMG)$_3$ precursor shows comparable thermal stability.[36] Hence, the NMR decomposition experiments suggest that, although the surrounding environment of these precursors in the bubbler and in the gas phase during the MOCVD/ALD process is certainly different from the one in the NMR tube, the lanthanide guanidinates **1** and **2** should be stable upon prolonged heating at evaporation temperature and not thermally decompose during the short ALD cycles, when introduced into the reaction chamber.

Thus considering the excellent thermal properties of **1** and **2** and taking their good solubility in common organic solvents (toluene, hexane, THF, diethyl ether etc.) in to account, one can conclude that these compounds are promising precursors for both thermal and liquid injection MOCVD of Gd_2O_3 and Dy_2O_3 thin films. In addition, due to the revealed extraordinary thermal stability, the presence of highly reactive M−N bonds and the higher basicity of the guanidinate ligand compared to the conventionally used β-diketonates, it can be expected that the rare-earth guanidinate complexes are very reactive toward OH functionalities, which will allow the use of H_2O as an oxygen source during ALD. This is confirmed by our preliminary studies on ALD of Gd_2O_3 thin films using the Gd(DPDMG)$_3$/H_2O process, where growth rates of about 1.1 Å/cycle in an relatively broad ALD window were observed.[36,64] A detailed ALD study of these two compounds will be published elsewhere.

(40) Kim, K. H.; Farmer, D. B.; Lehn, J.-S. M; Rao, P. V.; Gordon, R. G. *Appl. Phys. Lett.* **2006**, *89*, 133512.
(41) Niinisto, J.; Petrova, N.; Putkonen, M.; Niinisto, L.; Arstila, K.; Sajavaara, T. *J. Cryst. Growth* **2005**, *285*, 191.
(42) Duenas, S.; Castan, H.; Garcia, H.; Gomez, A.; Bailon, L.; Kukli, K.; Hatanpaeae, T.; Lu, J.; Ritala, M.; Leskelae, M. *J. Electocem. Soc.* **2007**, *154*(10), G207.

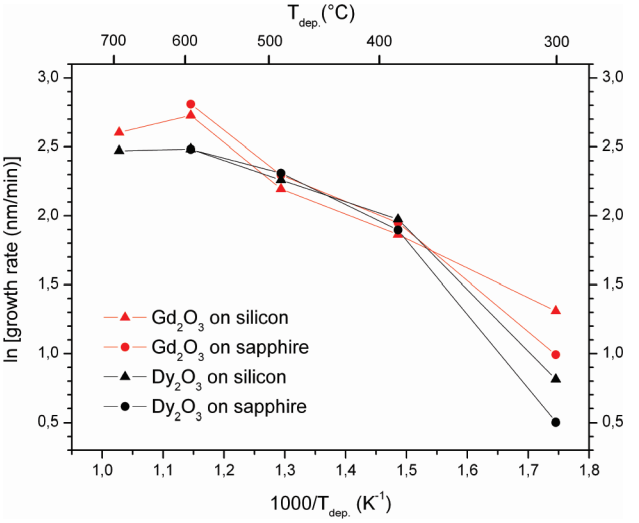

Figure 2. Arrhenius plot for the growth of Gd_2O_3 and Dy_2O_3 films deposited on Si(100) and Al_2O_3(0001) substrates using **1** and **2** as precursors.

In the following, the results on the MOCVD of Gd_2O_3 and Dy_2O_3 thin films using the *tris*-guanidinate precursors **1** and **2** will be presented. It should be noted that the main aim of the work was to prove the principle applicability of the precursors to grow the desired films under MOCVD conditions. We use a wide range of characterization methods (XRD, SEM, EDX, AFM, RBS, XPS, SNMS, $C-V$) to analyze the deposited Gd_2O_3 and Dy_2O_3 films, which allow us to study the deposition conditions vs film property relationships, recognize general trends and compare the results with those obtained using other Gd and Dy precursors. Beside providing a fundamental insight into the process physical and chemical characteristics, such an investigation is of undoubted importance in view of the future process optimization using state-of-the-art commercially available deposition equipment.

Precursor Performance. The performance of precursor **1** and **2** was tested by carrying out thin film deposition of Gd_2O_3 and Dy_2O_3 in a home-built thermal MOCVD reactor. The same set of experimental conditions viz. deposition time (15−30 min), carrier and reactive gas flow rates (50 sccm N_2; 50 sccm O_2), bubbler temperature (120 °C), and reactor pressure (1 mbar) were used for both the materials. Uniform Gd_2O_3 and Dy_2O_3 layers were deposited on Si(100) and Al_2O_3(0001) substrates in the temperature range 300−700 °C. The film growth rates were calculated using the layer thicknesses that were determined from the cross-sectional SEM measurements. The variation of the Gd_2O_3 and Dy_2O_3 growth rates with deposition temperature on different substrates is shown in Figure 2.

For the Gd_2O_3 depositions using Gd(DPDMG)$_3$ (**1**), a similar growth behavior on both Si(100) and Al_2O_3(0001) substrates is observed. The Arrhenius plot (Figure 2) shows a linear dependence of the growth rate on the substrate temperature in the 300−600 °C range, suggesting that the deposition is controlled by the kinetics of thermal decomposition of the precursor on the hot

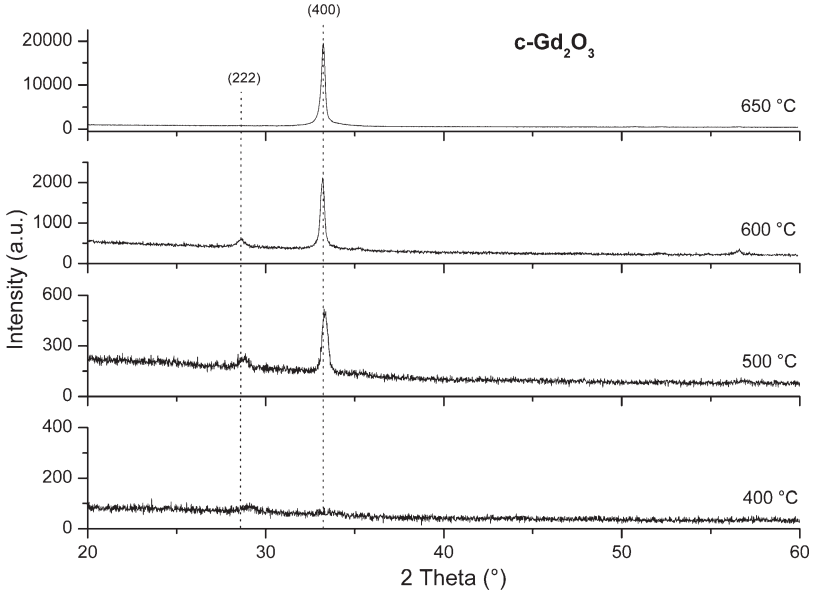

Figure 3. XRD diffraction patterns for Gd_2O_3 films deposited on Si(100) at 400−650 °C using $Gd(DPDMG)_3$ (**1**) (peak indexed according to JCPDS no. 43-1014).

substrate surface. The Gd_2O_3 growth rate on Si(100) reaches a maximum of 15.3 nm/min at 600 °C and than decreases to 13.5 nm/min at 700 °C, which is most probably due to thermal depletion of the precursor in the gas phase.

In contrast to growth rate behavior of Gd_2O_3 obtained from **1**, for the Dy_2O_3 films deposited using the analogous $Dy(DPDMG)_3$ precursor (**2**), the growth rate dependence on the deposition temperature is linear only in the temperature range between 300 and 500 °C (see Figure 2). Upon increasing the substrate temperature above 500 °C, saturation of the curve is observed, suggesting thus a diffusion-controlled growth regime.

Interestingly at 300 °C, the growth rate for Gd_2O_3 films deposited on sapphire (2.7 nm/min) is relatively lower than on silicon (3.7 nm/min). Similar growth rate dependence was also observed for the Dy_2O_3 depositions (1.7 nm/min on Al_2O_3; 2.3 nm/min on Si). A possible explanation for such growth rate behavior could be, e.g., a temperature difference on both substrates due to different thermal conductivities of silicon and sapphire; and/or higher thermodynamic barrier for thermal decomposition and nucleation on sapphire. Further, it is interesting to note that at 300 °C the growth rate for Gd_2O_3 on both substrates is slightly higher than the growth rate for Dy_2O_3 deposited under the same conditions. In the intermediate temperature range (400−500 °C), the growth rates for both Gd_2O_3 and Dy_2O_3 become comparable among each other, suggesting similar efficiencies for both precursors. At higher temperatures (600 °C) however, a significantly higher growth rate for the Gd_2O_3 is observed, which could probably be due to the different growth regimes that govern the MOCVD process.

Crystallinity and Morphology of Gd_2O_3 and Dy_2O_3. The crystallinity of the Gd_2O_3 and Dy_2O_3 thin films deposited in the temperature range from 300 to 700 °C using **1** and **2** as precursors was studied using powder XRD analysis.

As can be seen from Figure 3, the Gd_2O_3 films deposited at 400 °C were amorphous, whereas those grown above 400 °C were crystalline in nature. The reflections for the crystalline films could be indexed using the standard diffraction pattern for C-type cubic Gd_2O_3 (JCPDS no. 43-1014), which is the stable low temperature phase of this oxide.[43] For the Gd_2O_3 films grown at 500 and 600 °C, a low intensity (222) and a dominating (400) reflection are observed, suggesting that the films are polycrystalline with preferred (100) orientation. As the deposition temperature is raised, the intensity of the (400) reflection increases, suggesting an increased film crystallinity and a more pronounced (100) texture. Further increase in deposition temperature to 650 °C and above resulted in highly (100) oriented Gd_2O_3 films, as evidenced from the presence of the sole (400) reflection peak. It is interesting to note that while the Gd_2O_3 films grown on Si(100) using precursor **1** are highly (100) oriented, the Gd_2O_3 films deposited on the same substrate using $Gd(acac)_3$•Phen,[29] $[Gd(mmp)_3]_x$,[28] $[Gd(thd)_3]_2$,[44] and $[Gd(thd)_3]_x$•tetraglyme[27] were either polycrystalline or preferably (111) oriented. These differences could be attributed to difference in the physicochemical properties of the precursors and/or the different regimes controlling the film growth. For example, in the temperature range (400−600 °C), where using $[Gd(mmp)_3]_x$ and $[Gd(thd)_3]_x$•tetraglyme polycrystalline Gd_2O_3 films were deposited, a diffusion controlled growth takes place. In contrast, within the same temperature range, the Gd_2O_3 growth using precursor **1** is a kinetically controlled process.

As regards Dy_2O_3 (Figure 4), crystallization behavior comparable to Gd_2O_3 is observed. At lower deposition

(43) *Hanbook of Chemistry and Physics of the Rare Earth Elements*; North-Holland Publishing Company: Amsterdam, The Netherlands, 1982, Volume 5; Chapter 44.
(44) Lupak, R.; Fröhlich, K.; Rosová, A.; Hušeková; Ťapajna, M.; Machajdik, D.; Jergel, M.; Espinós, J. P.; Mansilla, C. *Microel. Eng.* **2005**, *80*, 154.

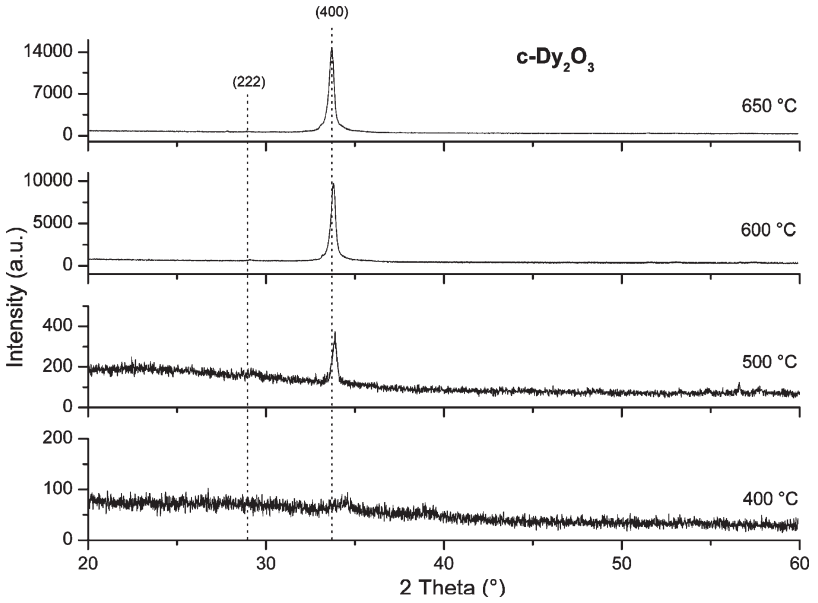

Figure 4. XRD diffraction patterns for Dy_2O_3 films deposited at 400−650 °C using $Dy(DPDMG)_3$ (**2**) (peak indexed according to JCPDS no. 43-1006).

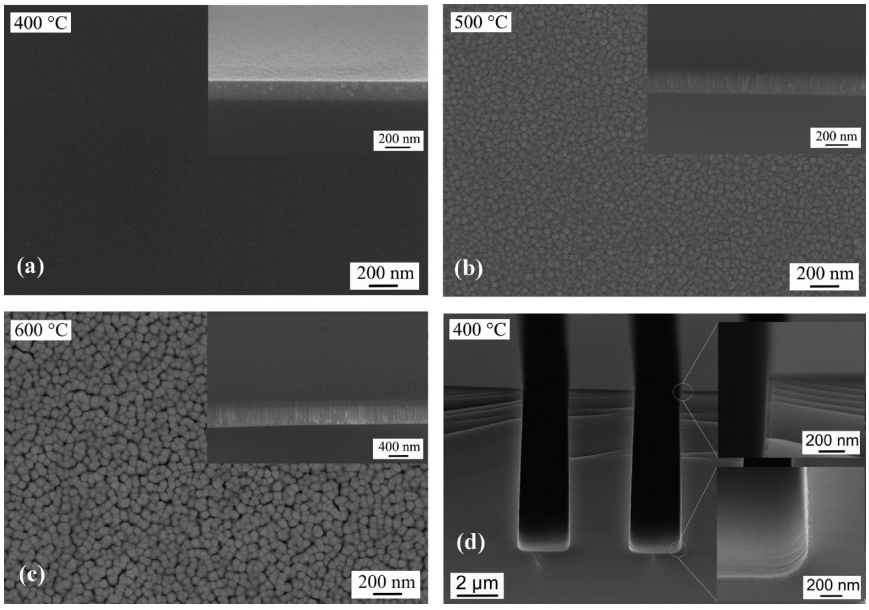

Figure 5. SEM micrographs of Gd_2O_3 films deposited on Si(100) at 400−600 °C (a−c) and a patterned Si(100) substrate at 400 °C (d).

temperatures the films are amorphous, showing no reflections in the diffraction pattern, whereas at higher temperatures C-type cubic Dy_2O_3 films are deposited (JCPDS no. 43-1006). In contrast to Gd_2O_3 however, the Dy_2O_3 films show even higher preference for the (100) orientation since the (222) peak that corresponds to a (111) orientation is very weak in intensity and only detectable for films grown at 500 °C. At higher temperatures, only the (400) reflection could indeed be observed, with an intensity increasing proportionally to the deposition temperature, suggesting a parallel increase in film crystallinity. In one of the very few previous reports on MOCVD of Dy_2O_3, where $Dy(EDMDD)_3$ was used as precursor, the LI-MOCVD (also referred as AVD) deposited films were polycrystalline in nature without any preferable orientation.[32]

The Gd_2O_3 and Dy_2O_3 film morphology as a function of deposition temperature was investigated using SEM analysis. Representative SEM micrographs of different Gd_2O_3 films grown on Si(100) substrates are presented in Figure 5.

Accordingly, the Gd_2O_3 film grown at 400 °C (Figure 5a) is smooth, without any distinct surface features. The cross-section image (shown as an inset) confirms its amorphous nature, since no defined grains and structure can be observed. An increase of the deposition temperature to 500 °C results in Gd_2O_3 film that consists of densely packed nanometer sized grains (5−40 nm). This is in accordance with the XRD results (Figure 3), where at 500 °C, a transformation from the amorphous to the crystalline phase was observed. As the substrate temperature is further increased to 600 °C, larger grains

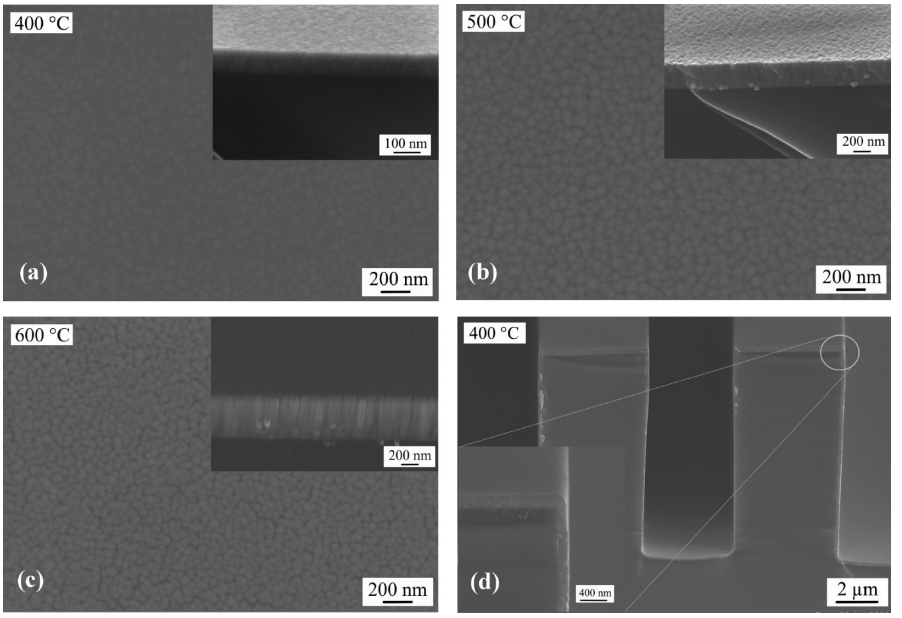

Figure 6. SEM micrographs of Dy_2O_3 films deposited on Si(100) at 400−600 °C (a−c) and patterned Si(100) substrate at 400 °C (d).

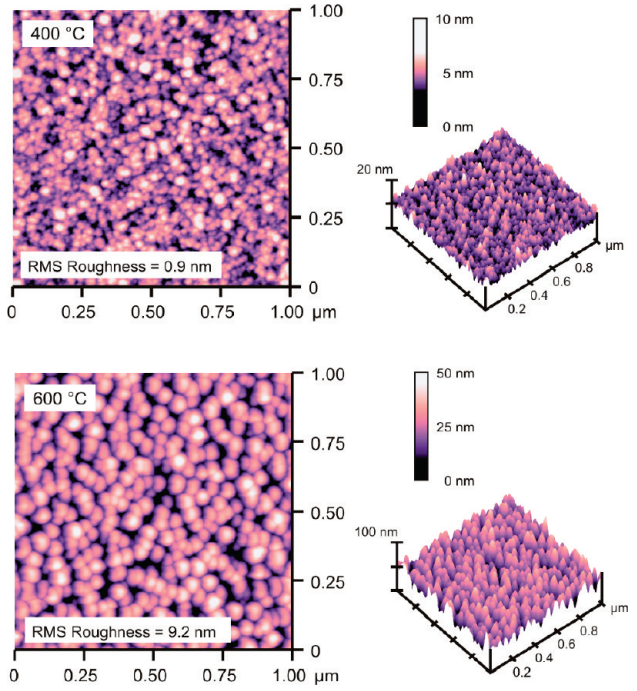

Figure 7. AFM micrographs of Gd_2O_3 films deposited on Si(100) at 400 and 600 °C (the micrographs are recorded in contact mode).

with well-defined boundaries and the presence of some voids on the sample surface become more apparent (Figure 5c). The observed circular domain size is typically on the order of 30−80 nm in diameter. The cross section of the 450 nm thick Gd_2O_3 film reveals a defined columnar structure with domains being up to 350−400 nm long. The increased grain size and the presence of some voids on the surface are probably due to the high deposition rate during the kinetically controlled growth attained at 600 °C, whereas the columnar structure of the film is in good agreement with its preferential growth in the (100) direction, as shown from the XRD analysis.

In order to prove the potential applicability of precursor **1** for the growth of Gd_2O_3 films on complex 3D geometries, depositions were also attempted on patterned Si(100) substrates (Figure 5d). It is seen that at a T_{dep} of 400 °C, the patterned substrate is uniformly coated with good step coverage. The film thickness is of the order of 110 nm on the top surface and decreases to 85 nm on the side wall at about 400 nm below the edge of the 8.5 μm deep trench. Further thickness decrease of more than 50% compared to the top surface was measured at the bottom of the trench and the close side walls, both having film thicknesses close to 42 nm. These observations clearly show that though on a flat substrate the kinetics of precursor decomposition governs the film growth (Figure 2), in the deep trenches of the patterned substrate this appears to be a diffusion controlled process. Nevertheless, the performed experiments show unambiguously that using precursor **1** a conformal coverage of complex 3D geometries is possible. However, additional process condition optimization needs to be carried out, if uniform film thickness over the entire substrate surface is required.

Representative SEM micrographs for Dy_2O_3 films deposited on Si(100) using $Dy(DPDMG)_3$ (**2**) are displayed in Figure 6 as a function of temperature. Though the Dy_2O_3 film grown at 400 °C (Figure 6a) appears to be slightly more structured compared to the featureless Gd_2O_3 deposited under the same conditions, the lack of reflections in the XRD pattern (Figure 4) and the dense, featureless structure observed in the cross section are clear indications for the predominantly amorphous nature of this film. As the deposition temperature is further increased, the morphological development is characterized by an increase in average grain size, caused by the crystallization of the films. Interestingly, the average grain size for the Dy_2O_3 film deposited at 500 °C is significantly larger than the grain size of the film deposited at 600 °C. This is in contrast to Gd_2O_3 depositions,

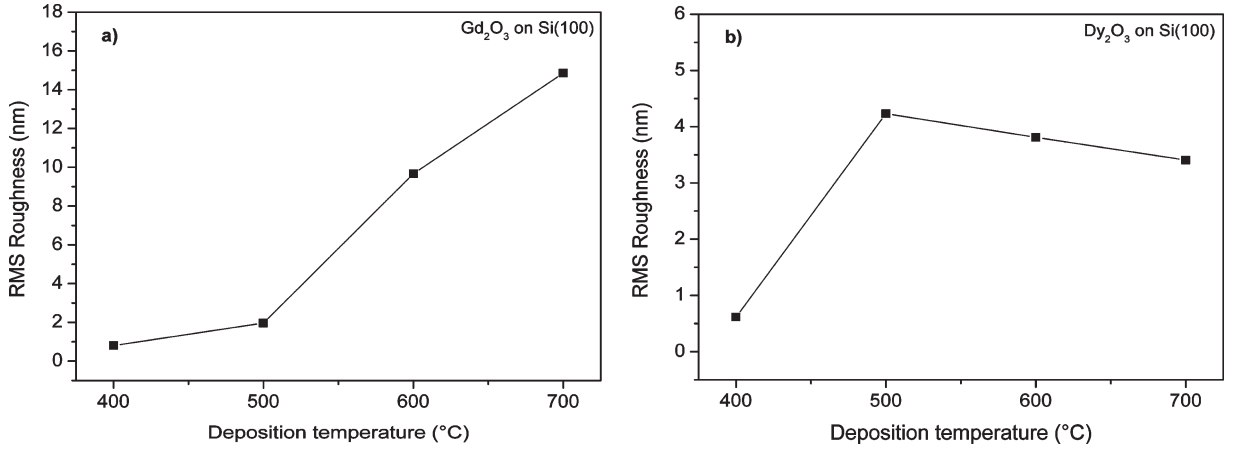

Figure 8. rms roughness vs deposition temperature curves for (a) Gd_2O_3 and (b) Dy_2O_3 films deposited on Si(100) substrates using **1** and **2** as precursors.

where grain size steadily increased with increasing deposition temperature. The observed variation in the morphology of the Dy_2O_3 and Gd_2O_3 films deposited at 500 and 600 °C is very likely due to the difference in the physicochemical processes involved during nucleation and growth of the films. In fact, as already discussed before, the Gd_2O_3 deposition is a kinetically controlled process up to 600 °C, whereas for Dy_2O_3 above 500 °C a diffusion dependent growth is observed.

As in the case of Gd_2O_3, the applicability of precursor **2** for the growth of Dy_2O_3 films on complex 3D substrate geometries was also investigated. Figure 6d shows that at 400 °C the patterned Si(100) substrate was successfully covered with a conformal Dy_2O_3 coating. Again, a significant difference in the film thickness at the top (250 nm) and the side wall (165 nm) of the trench was observed, indicating that in contrast to flat substrate, where the kinetics of precursor decomposition governs the film growth (Figure 2), in the deep trenches of the patterned substrate the Dy_2O_3 growth is a diffusion controlled process.

The morphology and surface roughness of the Gd_2O_3 and Dy_2O_3 films was further investigated using atomic force microscopy (AFM). It is important to note that the measurements on both materials were performed in different scanning modes. Although this should not affect the general trends in morphology and surface roughness dependence on deposition temperature, a direct comparison of the root-mean-square (rms) roughness values of Gd_2O_3 and Dy_2O_3 is only to be done with care. The variation of the rms roughness of the films with deposition temperature is depicted in Figure 8, and the AFM images of Gd_2O_3 and Dy_2O_3 films deposited at 400 and 600 °C are shown in Figures 7 and 9, respectively.

According to the AFM measurements, the surface of a 155 nm thick Gd_2O_3 film grown at 400 °C is smooth with an rms roughness of 0.9 nm (Figure 7). Upon increasing the deposition temperature up to 600 °C, a film of well-developed granular morphology was formed, with a significantly higher rms surface roughness (9.2 nm). The gradual increase in surface roughness of Gd_2O_3 with increasing deposition temperature revealed from the curve shown in Figure 8a is in good agreement with the XRD and SEM measurements, and, in particular, with the development of well crystallized and textured systems characterized by a marked granular topography for deposition temperatures higher than 500 °C.

The AFM surface analysis of the Dy_2O_3 thin films deposited under the same conditions as the Gd_2O_3 reveals a different dependence of surface roughness on the deposition temperature (Figure 8b). In common with Gd_2O_3, at a deposition temperature of 400 °C, the rms roughness value for 290 nm thick film is only 0.5 nm (Figure 9) but is strongly increased to more than 4 nm if a deposition temperature of 500 °C is applied. In contrast to Gd_2O_3, however, the surface roughness remains nearly unchanged when the deposition temperature is further increased above 500 °C. In accordance with XRD and SEM results, the sudden increase in roughness at 500 °C is probably caused by the crystallization of the film, whereas the nearly constant and even slightly decreasing roughness upon further increasing the deposition temperature could be due to change in growth mechanism that is clearly evident from the Arrhenius plot shown in Figure 2.

Composition of Gd_2O_3 and Dy_2O_3 Thin Films. The surface and in-depth chemical composition of Gd_2O_3 and Dy_2O_3 films deposited using **1** and **2** was investigated by the joint use of XPS, RBS, and SNMS.

Regarding XPS characterization, for both Gd_2O_3 and Dy_2O_3 layers very similar results were obtained irrespective of the deposition temperature, confirming thus a very similar chemical state of the lanthanide ions in the Ln_2O_3 films independent of the deposition conditions. As an example, representative photopeaks are reported in Figure 10 for two films deposited at 500 °C.

Both Gd 3d and 4d photoelectron peaks were characterized by a complex-shape signal, whose detailed attribution was not straightforward due to the fact that the pertinent literature is both very poor and controversial. The Gd 3d signal was dominated by the spin orbit components Gd $3d_{5/2}$ and Gd $3d_{3/2}$. The former, centered at BE = 1187.0 eV, agreed with some reports on Gd_2O_3, despite the fact that significantly higher values were also

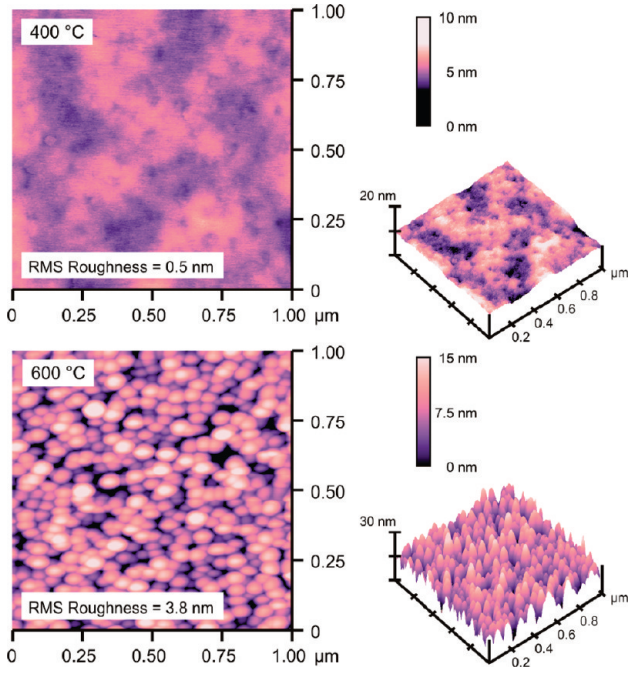

Figure 9. AFM micrographs of Dy_2O_3 films deposited on Si(100) at 400 and 600 °C (the micrographs of are recorded in tapping mode).

reported for the same system.[45−49] Similarly, the Gd $3d_{3/2}$ signal for the present sample was found at 1219.4 eV, in relatively good agreement with the work of Raiser et al.,[47] despite the fact that Söderlind et al.[48] reported a higher BE value. In addition, the weak satellites centered between the Gd $3d_{5/2}$ and Gd $3d_{3/2}$ components (BE = 1196.6 and 1207.7 eV) were likely attributed to energy-loss phenomena.[50,51]

In the case of the Gd 4d photopeak, a complex multiplet structure was observed, arising from electrostatic interactions between the 4d hole and 4f electrons.[52−54] Indeed, the overall photopeak was composed by an intense signal centered at a BE value of ca. 145 eV and a weaker satellite located ca. 30 eV higher. The former displayed the characteristic shape of a spin−orbit doublet, and their BEs [BE(Gd $4d_{5/2}$) = 142.1 eV; BE(Gd $4d_{3/2}$) = 147.5 eV] and spacing (Δ = 5.4 eV) were in agreement with some previous works on Gd_2O_3,[46,55,56] despite the fact that higher BE values for Gd(III) oxide have also been reported.[47,49,54,57] The satellite peak at BE = 170.3 eV was suggested to arise from exchange interactions.[56]

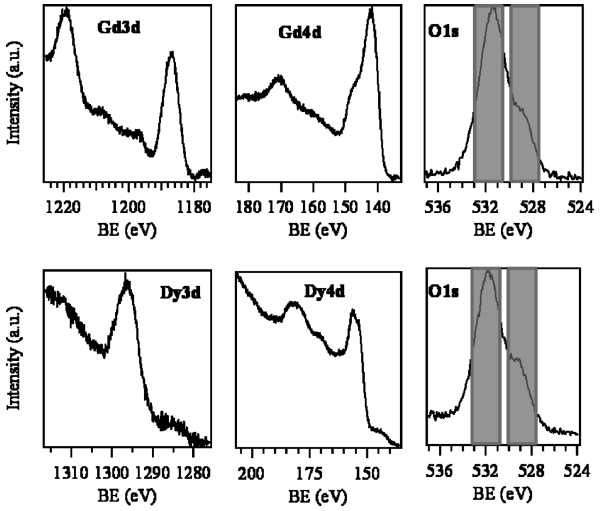

Figure 10. Representative surface XPS signals for Gd_2O_3 and Dy_2O_3 thin films deposited at 500 °C.

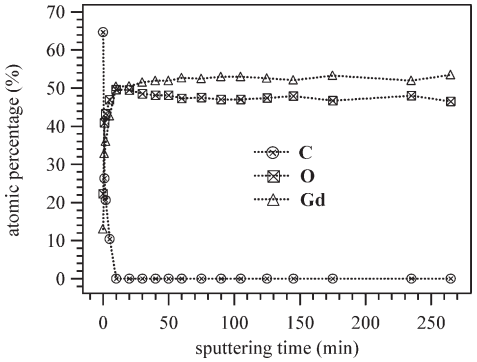

Figure 11. XPS depth profile for a Gd_2O_3 thin film deposited at 500 °C.

Concerning Dy, the Dy $3d_{5/2}$ peak was centered at BE = 1296.5 eV, an intermediate value between those previously reported for Dy_2O_3.[49,58,59] In analogy with the case of Gd 4d, even the Dy 4d signal displayed a complex profile attributed to final state multiplet coupling between the 4d hole and 4f electrons.[56] The overall photopeak consisted of an intense signal, with an absolute BE maximum of the main component at BE = 156.0 eV, and a broader and less intense feature at BE = 181.2 eV, with a shoulder at 170.4 eV. The two parts in the final state correspond to states with the 4d and 4f spins parallel and antiparallel. The absolute maximum of the main component was consistent with other investigations on Dy_2O_3.[46,56,60]

The calculated O/Gd(Dy) ratios were always exceeding the expected stoichiometric values for Gd_2O_3 and Dy_2O_3

(45) Hong, M.; Kortan, A. R.; Kwo, J.; Mannaerts, J. P.; Krajewski, J. J.; Lu, Z. H.; Hsieh, K. C.; Cheng, K. Y. *J. Vac. Sci. Technol.* **2000**, *B 18*, 1688.
(46) Uwamino, Y.; Ishizuka, T. *J. Electron Spectrosc. Relat. Phenom.* **1984**, *34*, 67.
(47) Raiser, D.; Deville, J. P. *J. Electron Spectrosc. Relat. Phemon.* **1991**, *57*, 91.
(48) Söderlind, F.; Pedersen, H.; Petoral, R. M., Jr.; Käll, P.-O.; Uvdal, K. *J. Colloid Interface Sci.* **2005**, *288*, 140.
(49) Sarma, D. D.; Rao, C. N. R. *J. Electron Spectrosc. Relat. Phenom.* **1980**, *20*, 25.
(50) Teterin, Y. A.; Teterin, A. Y.; Lebedev, A. M.; Ivanov, K. E. *J. Electron Spectrosc. Relat. Phenom.* **2004**, *137−140*, 607.
(51) Suzuki, C.; Kawai, J.; Takahashi, M.; Vlaicu, A.-M.; Adachi, H.; Mukoyama, T. *Chem. Phys.* **2000**, *253*, 27.
(52) Molle, A.; Perego, M.; Bhuiyan, M. N. K.; Wiemer, C.; Tallarida, G.; Fanciulli, M. *Appl. Phys. Lett.* **2007**, *90*, 193511.
(53) Gupta, J. A.; Landheer, D.; McCaffrey, J. P.; Spoule, G. I. *Appl. Phys. Lett.* **2001**, *78*, 1718.
(54) Zhou, J.-P.; Chai, C.-L.; Yang, S.-Y.; Liu, Z.-K.; Song, S.-L.; Chen, N.-F. *J. Cryst. Growth* **2004**, *260*, 136.
(55) Li, Y.-L.; Chen, N.-F.; Zhou, J.-P.; Song, S.-L.; Liu, L.-F.; Yin, Z.-G.; Cai, C.-L. *J. Cryst. Growth* **2004**, *265*, 548.
(56) Ogasawara, H.; Kotani, A.; Thole, B. T. *Phys. Rev.* **1994**, *B 50*, 12332.
(57) Terzieff, P.; Lee, K. *J. Appl. Phys.* **1979**, *50*, 3566.
(58) Paladia, B.; Lang, W.; Norris, P.; Watson, L.; Fabian, P. *Proc. R. Soc. Ser. A* **1977**, *354*, 269.
(59) Moulder, J.; Stickle, W.; Sobol, P.; Bomben, K. *Handbook of X-Ray Photoelectron Spectroscopy*; Perkin Elmer Corporation: Eden Prairie, MN, 1992.
(60) Craft, H.; Collazo, R.; Sitar, Z.; Maria, J. *J. Vac. Sci. Technol.* **2006**, *B 24*, 2105.

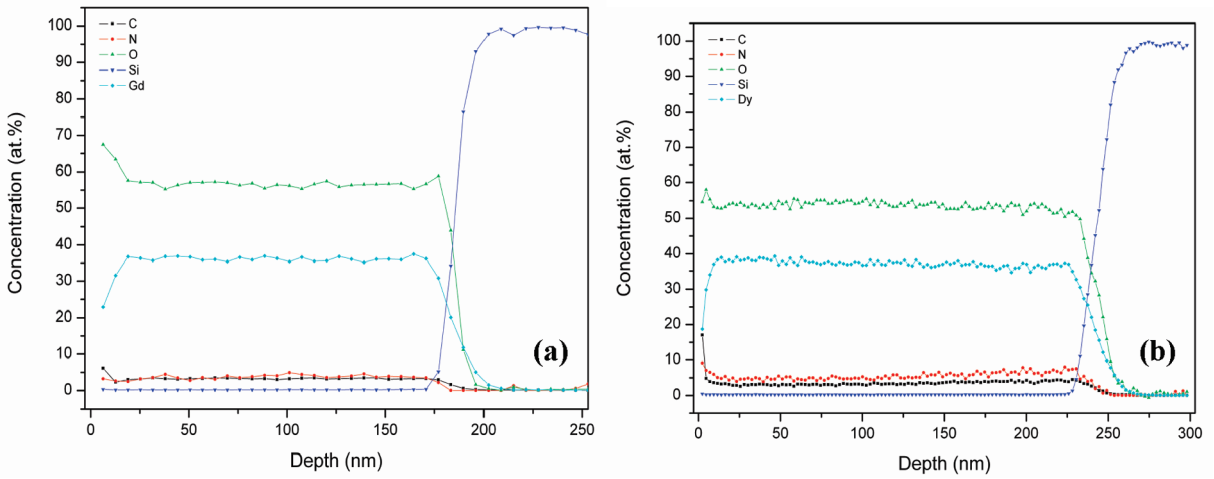

Figure 12. SNMS depth profiles of (a) Gd_2O_3 and (b) Dy_2O_3 thin films deposited at 450 °C on Si(100) using precursors **1** and **2**, respectively.

(1.5−2), suggesting that excess oxygen was present on the surface of the deposited films. In fact, for both Gd_2O_3 and Dy_2O_3 samples, the O1s band shape was characterized by two main components, highlighted in Figure 10 for the sake of clarity. The most intense contribution, centered at BE = 531.7 eV, was attributed to the presence of −OH groups and carbonates/bicarbonates, due to the high reactivity of lanthanides toward CO_2 and H_2O arising from atmospheric exposure.[44,46,55,59,61,62] The presence of carbonate species was indeed confirmed by a high BE shoulder centered at 288.4 eV in the C1s peak.[44,59,63] Appreciable amounts of hydroxide and carbonate functionalities have indeed been previously observed for both Gd_2O_3 and Dy_2O_3 thin films deposited by different methods (MOCVD, e-beam evaporation).[44,45,55,61,63] The minor O 1s component at BE = 529.1 eV was related to oxygen in $Gd(Dy)_2O_3$, despite the fact that the pertaining literature is rather ambiguous on lattice oxygen BEs.[45−47,49,54,55,57,59−61]

The predominance of the component attributed to −OH groups and carbonates/bicarbonates was not unexpected, due to the sample nanocrystalline structure and to its reactivity with moisture and CO_2 (see above). In fact, the presence of excess oxygen was previously observed in both LI-MOCVD and ALD deposited Gd_2O_3 films. For e.g. the O/Gd ratio for films LI-MOCVD grown using $[Gd(mmp)_3]_x$ as a precursor was 1.7−2.0,[28] whereas for ALD deposited films using $[Gd(thd)_3]_2/O_3$ and $(CpCH_3)_3Gd/H_2O$, this ratio was 1.8−2.4 and 1.6−1.8, respectively.[41] Nevertheless, for the present samples, sputtering treatments (5′, Ar^+ beam, 3 kV) resulted in a drastic intensity reduction of the high BE O 1s component at 531.8 eV, leading to an O/Gd(Dy) ratio close to 1.5, as expected for pure $Gd(Dy)_2O_3$.

In order to analyze the in-depth film composition, XPS depth profiling was undertaken. The obtained data are shown in Figure 11 for a representative Gd_2O_3 film. As can be noticed, the carbon atomic percentage rapidly decreases and falls to noise level after 10 min of Ar^+ sputtering, thus indicating that the deposited Gd_2O_3 is of good purity and that the detected carbon species mainly arise from atmospheric exposure and/or sample manipulation. As observed in Figure 11, concomitantly to the C decrease, the O and Gd percentages increase, both reaching a 50% value after 10 min of erosion. For longer sputtering times, a slight decrease of the oxygen percentage can be detected. This phenomenon can be attributed to preferential sputtering, whose occurrence is widely documented in the case of oxide-based materials.[38]

RBS analysis was further implemented to study the bulk properties of the Gd_2O_3 and Dy_2O_3 films. Accordingly, at high deposition temperature (600 °C), films are stoichiometric with O/Ln ratio of 1.51 ± 0.05 and 1.54 ± 0.05 for both Gd_2O_3 and Dy_2O_3, respectively. The slightly higher values at the deposition temperature of 450 °C might indicate differences in the MOCVD process characteristics under this condition. Looking closer at the RBS spectra (Supporting Information SI 3 and SI 4), one can see that in the case of the Gd_2O_3 the data deviate from the simulation of a homogeneous layer (red line) in the vicinity of the surface and the interface showing an overabundance of oxygen. This was also found from XPS and SNMS measurements (see below).

SNMS depth profiling was used to validate the data obtained from XPS and RBS and further investigate the film in-depth composition throughout the layer down to the interface to the substrate. The depth profiles of Gd_2O_3 (Figure 12a) and Dy_2O_3 films (Figure 12b) grown at 450 °C on Si(100) substrates show constant element distribution throughout the layers, indicating a very homogeneous film composition and sustainable MOCVD process.

(61) Jeon, S.; Hwang, H. *J. Appl. Phys.* **2003**, *93*(10), 6393.
(62) Kaltsoyannis, N.; Scott, P. *The f elements*; Oxford University Press: Oxford, 1999; Chapter 4.
(63) Frohlich, K.; Luptak, R.; Dobrocka, E.; Husekova, K.; Cico, K.; Rosova, A.; Lukosius, M.; Abrutis, A.; Pisecny, P.; Espinos, J. P. *Mat. Sci. Semicond. Proc.* **2006**, *9*, 1065.
(64) Milanov, A.; Xu, K.; Fischer, R. A.; Devi, A. Unpublished results.
(65) Potter, R. J.; Chalker, P. R.; Manning, T. D.; Aspinall, H. C.; Loo, Y. F.; Jones, A. C.; Smith, L. M.; Critchlow, G. W.; Schumacher, M. *Chem. Vap. Deposition* **2005**, *11*, 159.

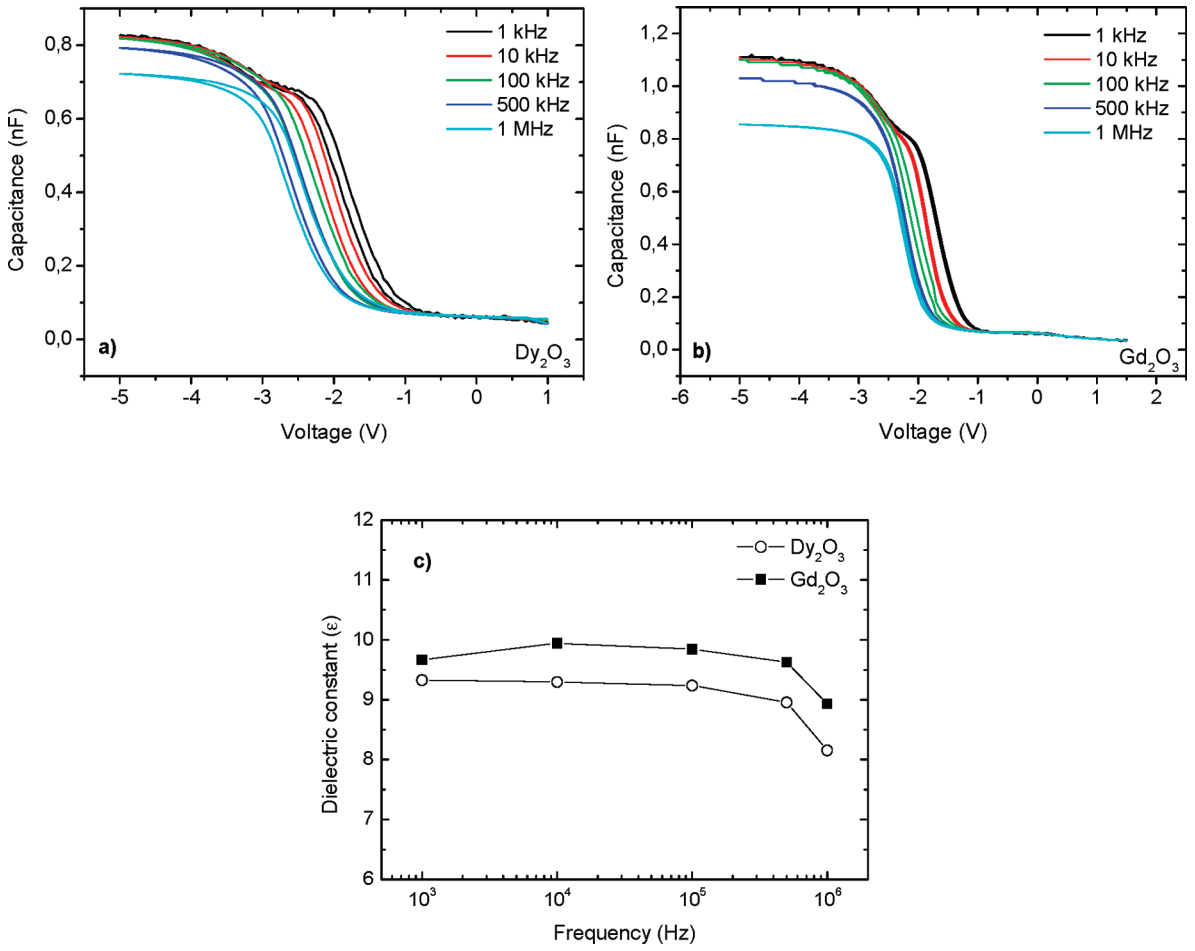

Figure 13. *C*−*V* curves measured at different frequencies for samples of (a) Dy_2O_3 and (b) Gd_2O_3grown at 400 °C. (c) Change in dielectric constant with AC frequency for films grown at 400 °C.

In accordance with the XPS surface analysis, large oxygen excess and significant carbon contamination are observed on the Gd_2O_3 surface, but after the removal of surface contaminations, nearly constant Gd and O concentration levels of 36 and 56 at % are obtained. This corresponds to O/Gd ratio of 1.56 which is good agreement with the ratio obtained from the RBS analysis (1.6, see Supporting Information SI 3). In addition, the presence of some carbon and nitrogen (ca. 3 at %) is detected throughout the film thickness. This is in contrast to the XPS depth profile, where no carbon or nitrogen contamination was observed. Thus, obviously other techniques such as nuclear reaction analysis (NRA) or elastic recoil detection analysis (ERDA) have to be used to quantify the concentration of the lighter elements in the films. Alhough, based on the present results, the actual existence, amount, and origin of the C and N contaminations is not clear so far, it is noteworthy to mention that, if indeed present, they could possibly be due to either implantation during sputtering or the inclusion of some undecomposed ligand fragments in the film at the relatively low deposition temperature of 450 °C. In the case of Dy_2O_3, after sputtering the highly contaminated surface, comparable levels of C and N are detected. On the basis of the Dy concentration of 35 at % and the O level of 53 at %, an O/Dy ratio of 1.51 is calculated which is in fair agreement with the RBS analysis (1.6, see Supporting Information SI 4).

Electrical Properties. Preliminary electrical investigations of the Gd_2O_3 and Dy_2O_3 films were carried out using a combination of *I*−*V* and *C*−*V* techniques. *C*−*V* measurements were recorded by sweeping a direct current (DC) bias superimposed on an alternating current (AC) signal of 1 MHz (and at 25 mV) from inversion to accumulation and back to inversion. Prior to any *C*−*V* studies, the leakage current through the MIS devices was measured. In this regard, typical leakage currents were found to be of the order of 10^{-11} A for both films under study; however, the leakage current is thickness dependent (the thicknesses of the Dy_2O_3 and Gd_2O_3 films in Figure 13 were 79 and 63 nm, respectively). Figure 13a and b shows *C*−*V* characteristics at different frequencies for films of Dy_2O_3 and Gd_2O_3 grown at 400 °C. It is evident that there is some variation in the capacitance of the materials with the AC signal, where the maximum capacitance decreases with an increase in frequency. Also noteworthy is the presence of a "hump" in the characteristics for both materials measured at <100 kHz, which then disappears as the frequency increases. The exact cause of the variation of accumulation capacitance with frequency is still being investigated; however, the observed systematic increase in the maximum capacitance

with decreasing AC signal frequency could be attributed to the presence of defect states (e.g., interface states, defects in the dielectric films), which are capable of following an AC signal only at lower frequencies. The higher values of accumulation capacitance at low frequencies could thus originate from the capacitance resulting from these defect states which is dependent on the relaxation time of the those states and the AC frequency. The relationship with frequency is also demonstrated in the observed reduction in dielectric constant (ε) at the highest frequencies (Figure 13c).

It can also be seen from Figure 13a and b that the $C-V$ curves for Gd_2O_3 are steeper in the region between accumulation and inversion and demonstrate negligible hysteresis when compared to those of Dy_2O_3. This suggests that the level of interface states (D_{it}) and mobile/fixed trapped charge is lower in the Gd_2O_3 layers than Dy_2O_3; however, these factors are currently under further investigation.

Summary

In this work, the feasibility of using the *tris*-guanidinato complexes Gd(DPDMG)$_3$ (**1**) and Dy(DPDMG)$_3$ (**2**) as precursors for the thermal MOCVD process to deposit Gd_2O_3 and Dy_2O_3 films has been successfully demonstrated. Conformal films with uniform thickness were deposited in the temperature range 300−700 °C on Al_2O_3-(0001) and Si(100), both as flat and as patterned 3D substrates. The effect of substrate temperature on the structural properties has been investigated. For the films grown in the temperature range 500−700 °C, an increase in crystallinity and a more pronounced (100) texture with increasing deposition temperature were observed. The films were stoichiometric, with carbon contamination merely limited to the outermost layers. As regards to dielectric properties, typical leakage currents were found to be of the order of 10^{-11} A for both materials. Due to the high thermal stability and excellent solubility of **1** and **2**, our current efforts are directed toward testing these precursors for ALD and LI-MOCVD applications. In addition, we are also evaluating the compatibility of these compounds with other rare-earth and transition metal precursors (Sc, Y, La, Hf, Ta, etc.) for the growth of complex oxide materials.

Acknowledgment. Dr. R. Neuser and Mr. M. Born are acknowledged for the SEM measurements. Dr. Martin Lemberger is acknowledged for supplying the patterned substrates. The funding supported by the German Science Foundation (DFG; CVD-SPP-1119) is gratefully acknowledged. A.P.M. and T.T. thank the Ruhr-University Bochum Research School and the Research Department IS^3/HTM of the Ruhr-University Bochum for the financial support.

Supporting Information Available: Evaporation rates of **1** and **2** in the temperature range of 100−160 °C, half life of **2** in solution at 100−220 °C, RBS spectrum of Gd_2O_3 deposited at 450 °C on Si(100) using **1**, and RBS of Dy_2O_3 deposited at 450 °C on Si(100) using **2**. This material is available free of charge via the Internet at http://pubs.acs.org.